JGR Atmospheres

RESEARCH ARTICLE
10.1029/2023JD038521

Nonlinear Response of Global Monsoon Precipitation to Atlantic Overturning Strength Variations During Marine Isotope Stage 3

X. Zhang[1,2], M. Prange[3], L. B. Ma[4,5], and J. Liu[6,7,8]

[1]School of Atmospheric Sciences, Nanjing University of Information Science and Technology, Nanjing, China, [2]Collaborative Innovation Center on Forecast and Evaluation of Meteorological Disasters (CIC-FEMD), Nanjing University of Information Science and Technology, Nanjing, China, [3]MARUM – Center for Marine Environmental Sciences, University of Bremen, Bremen, Germany, [4]CMA Earth System Modeling and Prediction Centre, Beijing, China, [5]State Key Laboratory of Severe Disaster, Chinese Academy of Meteorological Sciences, Beijing, China, [6]Key Laboratory for Virtual Geographic Environment, Ministry of Education, State Key Laboratory Cultivation Base of Geographical Environment Evolution of Jiangsu Province, Jiangsu Center for Collaborative Innovation in Geographical Information Resource Development and Application, School of Geography Science, Nanjing Normal University, Nanjing, China, [7]Jiangsu Provincial Key Laboratory for Numerical Simulation of Large-Scale Complex Systems, School of Mathematical Science, Nanjing Normal University, Nanjing, China, [8]Open Studio for the Simulation of Ocean-Climate-Isotope, Qingdao National Laboratory for Marine Science and Technology, Qingdao, China

Key Points:

- Nonlinear response of global monsoon rainfall to Atlantic Ocean circulation strength change in Marine Isotope Stage 3
- Simulated rainfall changes are consistent with reconstructed precipitation variations during millennial abrupt climate events
- Global monsoon rainfall is constrained by ocean heat transport

Supporting Information:

Supporting Information may be found in the online version of this article.

Correspondence to:

X. Zhang,
xzhang@nuist.edu.cn

Citation:

Zhang, X., Prange, M., Ma, L. B., & Liu, J. (2023). Nonlinear response of global monsoon precipitation to Atlantic overturning strength variations during Marine Isotope Stage 3. *Journal of Geophysical Research: Atmospheres*, *128*, e2023JD038521. https://doi.org/10.1029/2023JD038521

Received 17 JAN 2023
Accepted 5 OCT 2023

Author Contributions:

Investigation: M. Prange
Writing – original draft: X. Zhang
Writing – review & editing: X. Zhang, M. Prange, L. B. Ma, J. Liu

Abstract Monsoon rainfall proxy records show clear millennial variations corresponding to abrupt climate events in Greenland ice cores during Marine Isotope Stage 3 (MIS3). The occurrence of these abrupt climate changes is associated with Atlantic Meridional Overturning Circulation (AMOC) strength variations which greatly impact the global oceanic energy transport. Hence, the AMOC most likely plays a key role in modulating the global monsoon rainfall at millennial time scale. No modeling work has hitherto investigated the global monsoon system response to AMOC changes under a MIS3 background climate. Using the coupled climate model CCSM3, we simulated MIS3 climate using full 38 ka before present boundary conditions and performed a set of freshwater hosing/extraction experiments. We show not only agreement between modeling results and proxies of monsoon rainfall within the global monsoon domain but also highlight a nonlinear relationship between AMOC strength and annual mean global monsoon precipitation related to oceanic heat transport constraints. During MIS3, a weakened AMOC induces a decrease in annual mean global monsoon rainfall dominated by the northern hemisphere, whereas southern hemisphere monsoon rainfall increases. Above about 16 Sverdrups a further strengthening of the AMOC has no significant impact on hemispheric and global monsoon domain annual mean rainfall. The seasonal monsoon rainfall shows the same nonlinear response like annual mean both hemispherically and globally.

Plain Language Summary Approximately from 57 to 29 thousand years before present, fast warming events of around 10°C in Greenland temperature occurred on time scales of 1,000 years. The Atlantic Ocean circulation which transport heat northward could greatly impact global energy balance and a change in its strength is one plausible explanation for the occurrence of the warming events. The rainfall in monsoon regions also showed variations on the same time scale. So far, no study has investigated the linkage between monsoon rainfall and climate shift in high northern latitudes on such time scale with a specific background setup in a climate model. We show that ocean circulation change during the warming events could significantly impact global monsoon rainfall. When the ocean circulation slows down, northern/southern hemisphere monsoon rainfall decreases/increases linearly to circulation strength change. Interestingly, when the ocean circulation strengthens, monsoon rainfall in both hemispheres does not show obvious change. This nonlinear behavior is controlled by northward heat transport associated with the Atlantic Ocean circulation.

1. Introduction

The concept of "global monsoon" has been intensively studied during recent years either from a modern or paleoclimate perspective due to its great importance within the climate system and to human activities and livelihoods. From the paleoclimate community, different types of proxy records from various locations have been studied to examine monsoon rainfall variations over different time scales. Monsoon rainfall proxies have demonstrated

millennial scale monsoon oscillations globally (Cheng et al., 2012; Voelker, 2002). Such millennial variation in precipitation could be forced by climate condition change in the North Atlantic associated with abrupt climate shifts during the last glacial, namely, Dansgaard-Oeschger (D-O) events and ice melting events during Heinrich Stadials (HSs, Mohtadi et al., 2016; Y. J. Wang et al., 2001). D-O events featured fast (within decades or less) shifts from cold stadials to mild interstadials which lasted for several centuries in Greenland ice cores. These events were especially pronounced during Marine Isotope Stage 3 (MIS3, approx. 57–29 ka before present, X. Zhang & Prange, 2020). Heinrich Stadial 4 (HS4) occurred within MIS3 and was characterized by large iceberg-derived freshwater flux into the North Atlantic and a massive reduction of North Atlantic Deep Water (Elliot et al., 2001). The mechanisms behind millennial-scale monsoon variations and their linkage to high latitude forcing are still under debate and one potential candidate to explain such coupling process is the Atlantic Meridional Overturning Circulation (AMOC, Sun et al., 2012), which is responsible for more than half of the global oceanic heat transport toward high northern latitudes (Ganachaud & Wunsch, 2000).

One robust but incomplete picture shown in proxy records is that Northern Hemisphere (NH) summer monsoon was drier and Southern Hemisphere (SH) summer monsoon was wetter during HSs and D-O cold phases (Kanner et al., 2012; Y. J. Wang et al., 2008). During D-O cold phases and HSs, the AMOC slowed down (Elliot et al., 2002). SST in the North Atlantic along with Greenland surface temperature dropped dramatically (Schulz, 2002) whereas the SH surface temperature increased (Voelker, 2002). Such so called bipolar seesaw pattern could substantially change meridional temperature gradients, transport the signal from the North Atlantic to the low latitudes, push the Intertropical Convergence Zone (ITCZ) into the SH (warmer hemisphere) and led to a drier African, Asian and North American summer monsoon and a wetter South American and Indo-Australian monsoon (J. C. H. Chiang & Friedman, 2012; Mohtadi et al., 2016; Otto-Bliesner et al., 2014; Wen et al., 2016).

The AMOC is suggested to slow down in recent years (Praetorius, 2018) which might induce a bipolar seesaw and affect the monsoon rainfall. If this weaker AMOC continues to decrease in its strength, it might collapse and switch to an "off" mode (Hofmann & Rahmstorf, 2009; Prange et al., 2003). However, the future of the AMOC is highly uncertain and an increase in its strength cannot be ruled out either (Bakker et al., 2016). The global monsoon system in a stronger than present day AMOC situation has rarely been analyzed systematically although a persistently stronger AMOC could have existed during the last glacial cycle (Böhm et al., 2014). MIS3 serves as an ideal background climate to study the following questions due to its abrupt climate oscillations associated with AMOC strength variations: (a) How does the global monsoon rainfall respond to AMOC strength variations associated with forcing from the high latitudes? (b) Especially important, if the AMOC were to become stronger, how would the global monsoon rainfall be affected?

2. Experiment Design and Methods

The NCAR Community Climate System Model Version 3 (CCSM3, Collins et al., 2006; Yeager et al., 2006) is a full-complexity global general circulation model (GCM), which includes atmosphere, land, ocean and sea ice components. The atmosphere and land components share the T31 resolution in the horizontal (3.75°) and there are 26 vertical layers in the atmosphere and 10 soil layers in the land with activated dynamic vegetation module (Rachmayani et al., 2015). The ocean model has 25 vertical levels with layer thickness increasing from 8 m at the surface to around 500 m at the ocean bottom. The horizontal resolution is 3° at mid and high latitudes and around 0.9° around the equator with displaced North Pole over Greenland (Smith et al., 1995).

Using this model, we performed a 38 ka B.P. boundary condition control experiment, which represents the mid MIS3 period (referred to as MIS3 in the manuscript), and 12 freshwater hosing/extraction experiments with freshwater perturbation in the Nordic Seas. The freshwater perturbation amounts and experiment lengths are listed in Table S1 in Supporting Information S1. We use freshwater amount to refer to the specific sensitivity experiment, for example, +0.2 Sv test indicates we put 0.2 Sv freshwater into the Nordic Seas, whereas −0.2 Sv means we extract 0.2 Sv freshwater from the Nordic Sea surface. These model experiments applied different boundary conditions compared to present day, that is, sea level and land-sea distribution, greenhouse gas concentrations, orbital forcing (Figure S1 and Table S2 in Supporting Information S1) and continental ice sheets (Figure S2 in Supporting Information S1). All experiments were integrated long enough (>500 years) to reach new equilibria, which has been tested by a Student's *t*-test (i.e., trend in the AMOC strength time series is not significant for the last 100 years of each simulation). The applied positive and negative freshwater perturbations ranged from

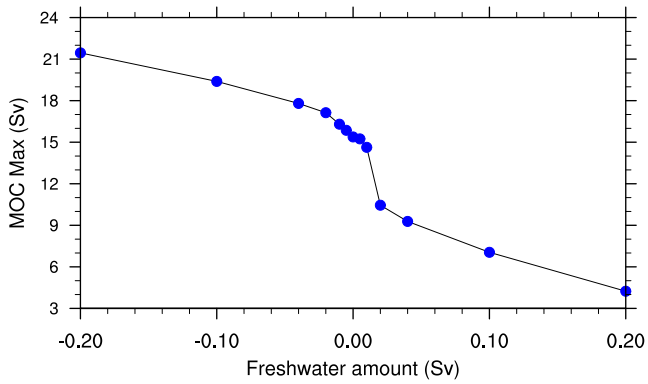

Figure 1. *Atlantic Meridional Overturning Circulation (AMOC) strength as a function of freshwater perturbation*. Positive/negative freshwater perturbation indicates freshwater input/extraction. The AMOC strength was defined as the maximum value of the overturning stream function below 300 m depth in the North Atlantic. Figure adapted from X. Zhang et al. (2014).

±0.005 Sv to ±0.2 Sv (1 Sv = 10^6 m^3/s). All analyses in this study are based on the last 100 years average from each experiment.

3. Results and Discussion

3.1. Nonlinear Response of AMOC Strength to External Freshwater Forcing

A nonlinear response was seen in AMOC strength in response to freshwater flux (Figure 1) as described before (X. Zhang et al., 2014). With positive freshwater forcing in the MIS3 North Atlantic, the strength of the AMOC decreased. A +0.2 Sv forcing is capable to cease the North Atlantic Deep Water Formation and the AMOC strength decreased from 15.38 to 4.24 Sv. Same amount negative forcing (−0.2 Sv) had weaker impact on the AMOC strength which resulted in an increase of the AMOC strength from 15.38 to 21.45 Sv. We interpreted the weak AMOC state as cold stadials and strong circulation as mild interstadials in this study. Greenland surface temperature and NH winter sea ice cover also showed nonlinear shape as a function of freshwater perturbation (not shown here). Such abrupt change in temperature and ice cover was related to observed D-O events during MIS3 (X. Zhang et al., 2014) and the +0.2 Sv hosing experiment is interpreted as a simulation of HS4. The asymmetry in AMOC-freshwater response (e.g., limited change in AMOC strength in response to negative freshwater flux vs. stronger reduction in AMOC in response to positive freshwater flux) is seen in models of different complexity. Hofmann and Rahmstorf (2009) tested the sensitivity of the AMOC to freshwater injection latitude, advection scheme and mixing parameterization in an intermediate complexity coupled model. Their results showed similar asymmetry regardless of model setup since salt advection dominates the circulation. The AMOC strength was positively correlated to maximum mixed layer depth in the North Atlantic but increasing freshwater extraction was not able to significantly affect the former. Using a more complex coupled GCM, Jackson and Wood (2018) showed that the method of freshwater injection does not impact hysteresis either. The AMOC stayed at a constant rate as negative freshwater increased due to a surface salinity constraint. As we extracted freshwater in the North Atlantic, the AMOC became stronger. Consequently, it transported more energy to the NH mid and high latitudes and led to higher salinities and temperatures at surface and intermediate depths there. However, with stronger AMOC the evaporative subtropical Atlantic becomes fresher due to relatively low-salinity inflow from the south, such that the salt transport from the subtropics to the high northern latitudes "saturates" for strong AMOC, which makes it more difficult to further speed up the AMOC with freshwater extraction.

3.2. Nonlinear Response of Global Monsoon Precipitation and ITCZ Latitude to AMOC Strength Change

Freshwater forcing did not affect the AMOC strength symmetrically in our model runs. More importantly, both seasonal and annual global monsoon precipitation also show a nonlinear response to AMOC strength. Figure 2a shows annual mean precipitation in the MIS3 control run.

The global monsoon domain (red contour) was defined using the following criteria (P. X. Wang et al., 2014; Y. J. Wang et al., 2008): (a) annual mean local summer (May to September in NH, November to March in SH) minus winter (May to September in SH, November to March in NH) precipitation is greater than 300 mm and (b) local summer precipitation exceeds 55% of annual total rainfall. Compared to present day conditions, the monsoon domain generally retreated in the north and expanded to the south over land due to decreased summer to annual precipitation ratio in a colder climate (Yan et al., 2016; Figure 2a). We note however, that the global monsoon domain is not the focus of this study since the area of the global monsoon domain does not vary much over all the model experiments.

The global monsoon region annual averaged rainfall rate is 3.43 mm/day in MIS3. When the AMOC decreased to 4.24 Sv during HS4 in the model, local summer monsoon precipitation was generally reduced in the north and increased in the south. The strongest change in boreal summer monsoon precipitation was observed in tropical America and the tropical North Atlantic Ocean, featuring more than 3 mm/day precipitation decrease. The central equatorial Atlantic experiences maximum rainfall increase, which is larger than 3 mm/day. The Asian monsoon

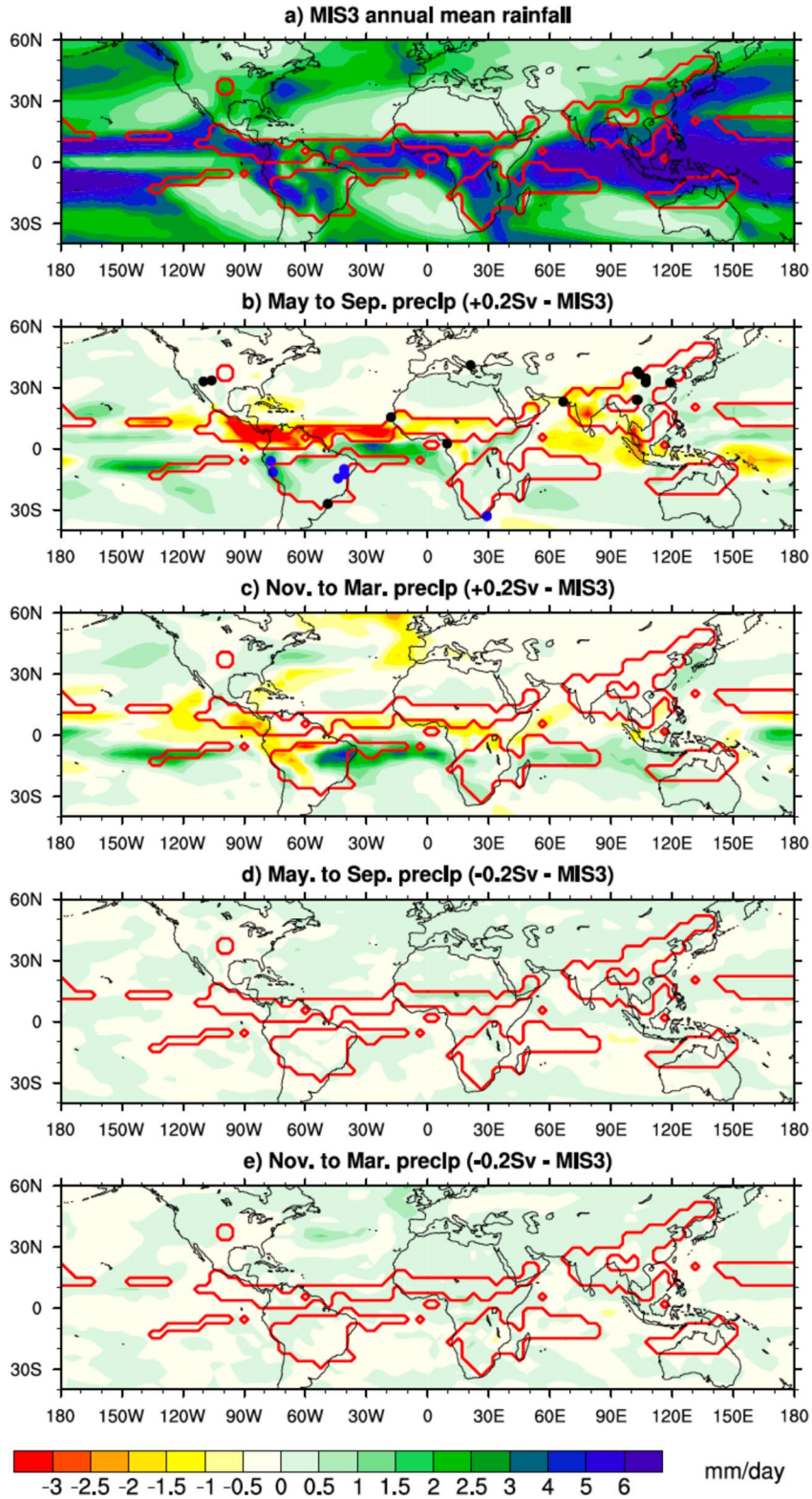

Figure 2. *Annual total precipitation and anomalies between different experiments*. (a) Marine Isotope Stage 3 (MIS3) control run; (b) difference between +0.2 Sv experiment and MIS3 control run during May to September; (c) difference between +0.2 Sv experiment run and MIS3 control run during November to March; (d) difference between −0.2 Sv experiment and MIS3 control run during May to September; and (e) difference between −0.2 Sv experiment and MIS3 control run during November to March. Red contour area indicates the global monsoon region calculated by modeled rainfall data. Dots in panel (b) are the proxy record locations as it is discussed in Section 3.3. Black indicates drier summer monsoon and blue indicates wetter summer monsoon.

rainfall generally decreases especially over southeast Asia (Figure 2b). During boreal winter, the strongest rainfall change moves southward over the Pacific and the Atlantic associated with the seasonal shift of the ITCZ and a strong rainfall increase is simulated over Northeast Brazil (Figure 2c).

In the case that AMOC strength increased to 21.45 Sv in the −0.2 Sv experiment, the monsoon precipitation responded generally oppositely and about one order of magnitude weaker compared to the +0.2 Sv run in boreal winter and summer. The most significant increase in rainfall was observed in the African monsoon region in boreal summer (Figures 2d and 2e).

The statistical significance (at 95% confidence level) of the surface temperature differences between the ±0.2 Sv runs and the MIS3 control run, calculated using a *t*-test, is shown in Figure 3. The same test is applied for surface wind differences. In the +0.2 Sv experiment, during May to September, Northern Indian Ocean surface temperature slightly decreased and continental surface temperature increased, which resulted in a stronger meridional temperature gradient and westerly wind anomalies, thus strengthening regional summer monsoon surface flow. Weaker monsoon winds were observed over East Asia and western Africa associated with weaker land-ocean temperature contrasts compared to the unperturbed MIS3 control run. The wind anomalies blew toward the Australian continent, indicating a weaker local winter monsoon surface wind (Figure 3a). As for November to March, wind anomalies were directed away from the continent in the East Asian and African monsoon regions whereas over Australia, a northwest wind anomaly was seen. However, temperature and wind changes in northern Australia were not significant (Figure 3b).

For an AMOC stronger than the MIS3 baseline state, simulated winds and temperatures showed changes generally in opposite direction compared to weaker AMOC condition. Global monsoon surface flow became generally stronger in boreal summer and weaker in boreal winter. However, with the same magnitude of freshwater perturbation (−0.2 Sv), the monsoon responses were much weaker. Between May and September, most of the SH ocean experienced a cooling of less than 1°C and NH warming was generally seen only above 20°N with maximum of around 3°C in the central North Atlantic. Surface wind change was less than 1 m/s (Figure 3c). During November to March, NH warming was slightly stronger than in boreal summer in mid and high latitudes over the North Atlantic and surface wind change had a similar pattern as during May to September in the monsoon regions (Figure 3d).

The annual mean precipitation in the global monsoon domain decreased rather linearly when the AMOC strength was below 15.38 Sv but kept at a steady level at around 3.4 mm/day when we imposed negative forcing in the Nordic Seas (Figure 4a). The mean ITCZ latitude (defined as the median latitude of maximum annual mean precipitation between 20°N and 20°S) was constantly around 0.3°N when the AMOC increased from 15.38 to 21.45 Sv, but it moved southward and reached the SH with decreasing AMOC strength. Separating local summer and winter precipitation in the NH and SH gave a quite similar figure. In both hemispheres, local summer and winter monsoon precipitation no longer significantly increases or decreases when the AMOC reaches ca. 16 Sv. However, in both seasons, monsoon precipitation decreased linearly in the north and increased in the south when the AMOC strength decreased with positive freshwater forcing (Figures 4b and 4c). The NH monsoon rainfall dominated the annual mean global monsoon rainfall since the north experiences significant drying when the ITCZ moved southward in response to AMOC weakening.

3.3. Model-Proxy Data Comparison of Global Monsoon Precipitation During MIS3

There are only a few rain-related proxy records spanning MIS3 allowing to reconstruct monsoon precipitation variability on millennial time scale (An et al., 2015). They all demonstrated a linkage between AMOC strength related abrupt climate shifts and monsoon precipitation. Though interpretation of oxygen isotopes ($\delta^{18}O$) is still under debate, theoretical and empirical studies support the idea that lower isotope values are associated with wetter summer monsoon globally, especially in the Asian monsoon region (e.g., Cheng et al., 2009; C. H. Chiang et al., 2015; Orland et al., 2015). There are several such records from South American sites at Botuvera (X. Wang et al., 2006, 2007), Peru (Cheng et al., 2013), Pacupahuain Cave (Kanner et al., 2012), Bahia State (X. Wang et al., 2004), and central eastern Brazil (Stríkis et al., 2018). All these data showed a more humid South America when the NH was cooler connected to iceberg melting events in the North Atlantic during HSs.

In the Asian monsoon region, oxygen isotopes from Hulu cave (Y. J. Wang et al., 2001) and Songjia cave (Zhou et al., 2014) varied out-of-phase with records from South America above. A sharp increase in $\delta^{18}O$ during HSs represented a weaker and drier east summer Asia monsoon during the NH cold phases. Meanwhile, two records from the Indian Monsoon region, Xiao Bailong Cave ($\delta^{18}O$ from Cai et al. (2006)) and Arabian Sea sediment core

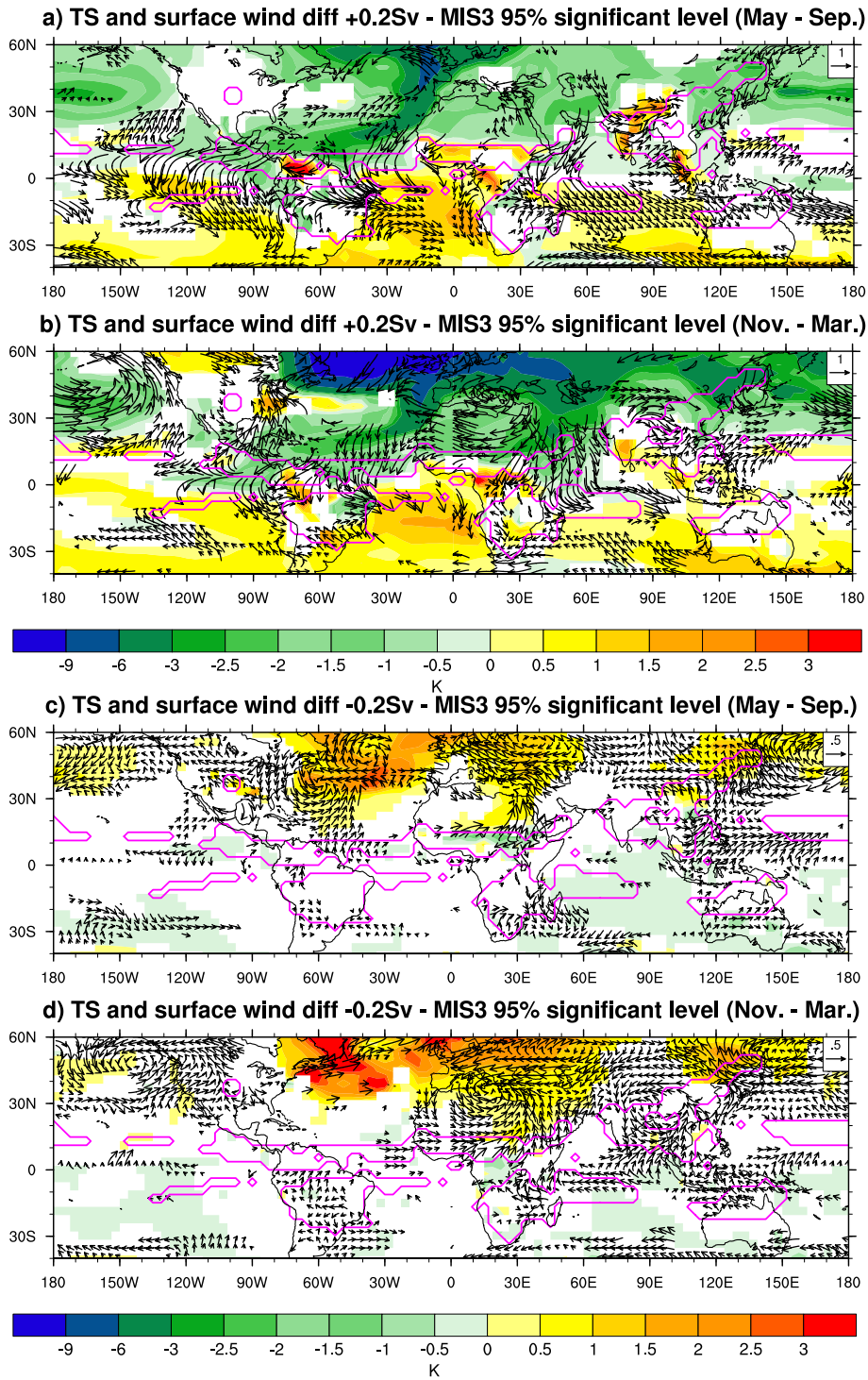

Figure 3. *Surface wind and surface temperature differences*. (a) May to September difference between +0.2 Sv experiment and Marine Isotope Stage 3 (MIS3) control run; (b) November to March difference between +0.2 Sv experiment and MIS3 control run and; (c) same as panel (a) but for the −0.2 Sv experiment; and (d) same as panel (b) for the −0.2 Sv experiment. Wind difference vector unit: meter per second. Values above 95% confidence level are shown. Pink contour area indicates the global monsoon region as the same in Figure 2.

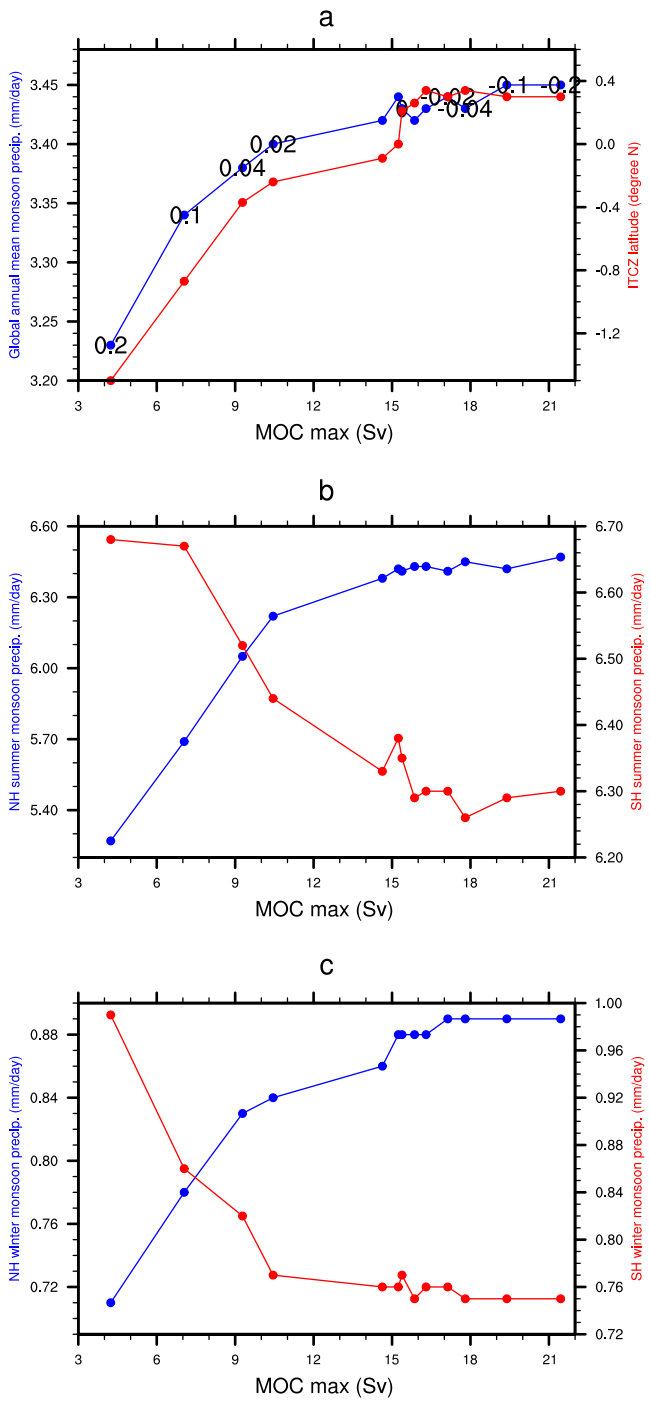

Figure 4. *Climate responses to Atlantic Meridional Overturning Circulation (AMOC) strength change*. (a) Mean Intertropical Convergence Zone latitude and annual mean precipitation rate in global monsoon region as indicated in Figure 3 as a function of AMOC strength; (b) average summer (May to September for Northern Hemisphere [NH] and November to March for Southern Hemisphere [SH]) precipitation rate in global monsoon region as a function of AMOC strength in the two hemispheres; and (c) same as (b) but for hemispheric winter (November to March for NH and May to September for SH).

SO130-289KL (sediment reflectance from Deplazes et al. (2016)) indicated a drier Indian summer monsoon during the cold stadials. Several lake records over land from east and south Asian monsoon regions, which are sensitive to millennial monsoon rainfall change also demonstrated drier conditions during the HSs (^{10}Be from Beck et al. (2018); Ca/K and Fe/K ratios from Sun et al. (2021) and sediment analyzes from Zhao et al. (2020)). Loess records highlighting millennial scale rainfall variation and monsoon weakening during the stadials are also presented in several studies including elemental ratios (Guo et al., 1996; Sun et al., 2021), carbonate carbon isotopes (Sun et al., 2019), and microcalcareous oxygen isotopes (Z. Zhang et al., 2022). Moreover, bulk Fe/K ratios from the north African monsoon region (marine sediment core GeoB9508-5, Mulitza et al., 2008) correlating with oxygen isotope values in the NGRIP ice core (Andersen et al., 2004) showed arid conditions during the HSs, whereas higher Fe/K ratios in core CD154-17-17K indicated more humid south African conditions during the same intervals (Ziegler et al., 2013). Overall, millennial-scale resolution proxies in the two hemispheres varied anti-phased with each other in response to millennial-scale North Atlantic condition changes. An abrupt cooling in the North Atlantic surface corresponds to a weakening of NH summer monsoon and an intensified SH summer monsoon and vice versa. Such dipole pattern change in monsoon precipitation is associated with an AMOC-driven southward shift of the ITCZ and more asymmetric Hadley cells during the HSs. Most of the oxygen isotope records showed 2–3‰ differences comparing the cold HSs with warm interstadials, indicating a drop in seasonal precipitation in the NH and an increase in the SH. Xiao Bailong cave record experienced an especially strong change in the δ^{18}O signal, implying a significant weakening of the Indian summer monsoon when the AMOC was presumably weaker (Cai et al., 2015).

In our simulation results, for all records within the global monsoon region, model results are consistent with most of the reconstructions, featuring enhanced SH summer monsoon rainfall and drier NH summer monsoon during the HSs. However, the model produced drier conditions during austral summer in western South America. Hence, at two sites (Pacupahuain cave and north Peru) the model showed less precipitation during HS4, which seems to contradict the proxy records. The reconstructed enhanced precipitation could also be related to austral winter precipitation, as previously suggested (Campos et al., 2019). Though at Hulu cave location (within the South Asian Monsoon region), summer monsoon precipitation slightly increased during HS4 which is inconsistent with the proxy record, the simulated Indian monsoon precipitation is largely reduced in the HS4 experiment compared to the MIS3 control run. It should be noted that model-data comparison in this study only aims at verifying simulated rainfall change between stadials and interstadials. The proxy records do not allow validation of the modeled nonlinearity. Recent studies have suggested that δ^{18}O records do not correlate well with either local precipitation amount or local temperature at reconstruction sites. Variation of δ^{18}O values could reflect processes that are independent of rainfall (e.g., J. C. Chiang et al., 2020). However, oxygen isotope records mentioned in this manuscript were all interpreted as precipitation in the corresponding studies.

3.4. Mechanism of Global Monsoon Precipitation and ITCZ Change as Response to AMOC Strength Variation

The monsoon-ocean coupled system is influenced by tropical SSTs and polar ice (Pierrehumbert, 2000; Webster, 1994). The AMOC can affect both by redistributing ocean heat content. A weaker AMOC, less northward oceanic heat transport, larger sea ice cover and colder surface temperature

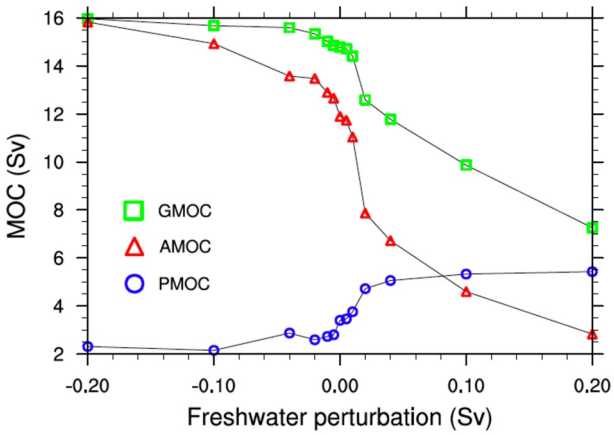

Figure 5. *Cross equator meridional overturning circulation strength as a function of freshwater perturbation*. Circulation strength was defined as the maximum of streamfunction in the ocean below 400 m at the equator. Green square is global, red triangle is Atlantic, and blue circle is Pacific. Note: Atlantic Meridional Overturning Circulation in Figure 1 indicates maximum of streamfunction in the ocean below 300 m in whole North Atlantic.

in Greenland is associated with D-O cold phases and vice versa. D-O event signals could be found in the tropics over the monsoon region (X. Zhang et al., 2015). The spread of their impact from the high latitudes to the tropics due to AMOC strength variations could be a plausible explanation of millennial scale global monsoon variability as it is observed in the proxy records. Taking the +0.2 Sv freshwater hosing experiment as an example, the AMOC strength significantly decreased mimicking the effect of melted ice which has greatly reduced North Atlantic Deep Water Formation during HS4. North Atlantic surface temperatures dropped by more than 20°C at high latitudes since the freshwater decreased ocean shallow layer salinity and hampered convection. A bipolar seesaw pattern was shown due to less oceanic heat transport to the north (Stocker & Johnsen, 2003) and amplifying feedbacks like a higher albedo. The temperature seesaw also led to a specific humidity seesaw in the model featuring less atmospheric water vapor in the north, while the SH became wetter. Moreover, a colder NH led to stronger subsidence and a warmer SH favored uplifting of moist air in the tropics. Therefore, the NH/SH summer monsoon rainfall was reduced/increased. The above process became stronger when we put more freshwater into the North Atlantic as it is shown in Figure 4. The opposite (D-O warm phase) is true for a stronger AMOC. The NH became warmer and wetter which led to more monsoon rainfall. By contrast, the SH became cooler, drier and the monsoon rainfall was reduced. As a result, the ITCZ moved to the warmer hemisphere. A similar surface temperature seesaw and southward shift of the ITCZ in hosing experiments were shown under pre-Industrial and Last Glacial Maximum conditions performed by atmosphere-ocean general circulation models and ITCZ latitude changes were attributed to enhanced/weakened NH/SH Hadley cells (J. Chiang et al., 2003; R. Zhang & Delworth, 2005). However, intermediate complexity model simulations did not show changes in ITCZ location due to simplified atmospheric dynamic processes (e.g., Stouffer et al., 2006).

Above a certain threshold (ca. 16 Sv), the global cross equator oceanic heat transport does hardly increase though the AMOC strengthened. This can partly be attributed to a compensating effect of the Pacific Meridional Overturning Circulation (PMOC, defined as maximum meridional ocean streamfunction in the Indo-Pacific basin below surface level), which increases with decreasing AMOC (Figure 5). This Atlantic–Pacific overturning seesaw has been described in previous studies and attributed to a positive feedback between ocean circulation and salinity contrasts (Saenko et al., 2004). Consequently, cross equator oceanic heat transport changes in the Pacific and Atlantic partly compensated each other over a wide range of freshwater forcing, such that the global cross equatorial heat transport became almost steady (Figure 6). A weaker AMOC transports less heat to the NH which was indemnified by more northward heat in the Pacific. Since net radiation at the top of the atmosphere is almost identical in the northern and southern hemispheres, a change in cross equator oceanic heat transport could affect the low latitude mean atmospheric circulation pattern (Frierson et al., 2013). Reduced northward oceanic heat transport is thus associated with enhanced atmospheric heat transport across the equator. The atmospheric transport even changed its direction from southward to northward (Figure 7).

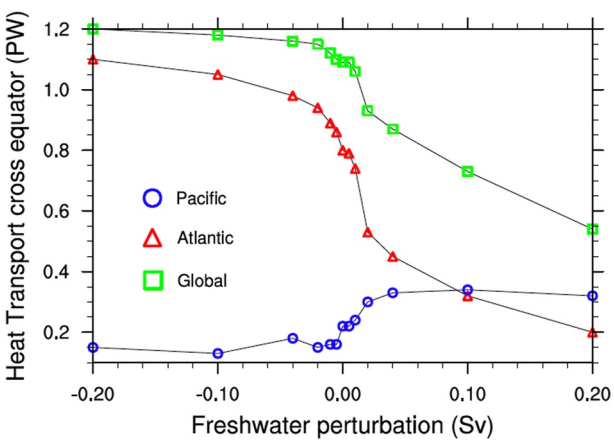

Figure 6. *Cross equator heat transport as a function of freshwater perturbation*. Green square is global, red triangle is Atlantic, and blue circle is Pacific.

The changes in the cross equatorial atmospheric heat transport are accomplished by reorganizations of the Hadley circulation. The Hadley cell became weaker in the SH and stronger in the NH in the HS4 (+0.2 Sv) run since the temperature seesaw induced anomalous surface southward flow at the equator. Associated northward atmospheric heat transport also increased (Figures 8a and 8c). Corresponding to the shift of the rising branch of the Hadley cell, the mean ITCZ stayed in the SH and the annual mean rainfall within the global monsoon domain decreased. The opposite is true in the −0.2 Sv test since the tropical atmosphere transported heat to the south (Figures 8b and 8d).

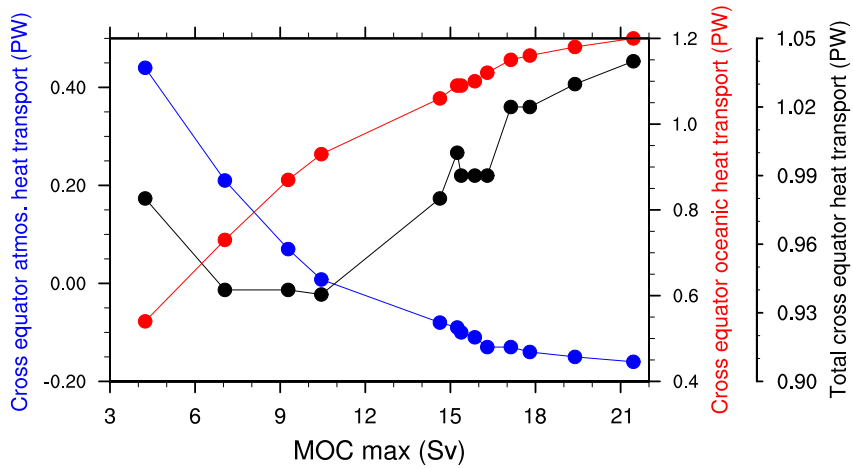

Figure 7. Global cross equatorial oceanic, atmospheric, and total heat transports as a function of Atlantic Meridional Overturning Circulation strength.

The annual mean rainfall in the global monsoon domain did not further increase and the ITCZ stayed around 0.4°N when the AMOC strength reached ca. 16 Sv and above. Corresponding to the southward shift of ITCZ when the AMOC slows down, the tropical meridional SST gradient became sharper between the two hemispheres. The asymmetrical monsoon precipitation response is constrained by a nonlinearity in oceanic and atmospheric heat transport as it is shown in Figure 7. Beside the heat transport constraint other components in the climate system that influence monsoons and exhibit nonlinear behavior can add to the nonlinear global monsoon response, in particular sea ice. A stronger AMOC reduces North Atlantic sea ice cover until a minimum is reached beyond which there is almost no sea ice response to further AMOC increase (X. Zhang et al., 2014) and hence no further sea ice effect on the global monsoon. An increase of sea ice in HS4 could reduce ocean convection and have more significant impact on the global monsoon.

To further investigate monsoon rainfall and circulation changes in individual monsoon domains, 1,000–500 hPa water vapor flux along with 500 hPa vertical velocity in the ±0.2 Sv experiments was compared with the MIS3 control run. The MIS3 control experiment showed strong water vapor convergence toward individual local summer monsoon domains accompanied by upward motion (Figures 9a and 9b). In the +0.2 Sv case during boreal summer, anomalous water vapor transport was directed away from Asian and African monsoon regions accompanied by weaker upward motion (except eastern part of Asia) whereas in the SH, more water vapor was transported toward the monsoon regions and vertical motion was strengthened (Figure 9c). Decreased summer monsoon rainfall over Indonesia was associated with weakening and southward shift of the Walker circulation in southern Pacific and further reduced Indian summer monsoon through Rossby wave propagation (Lau & Nath, 2000). R. Zhang and Delworth (2005) found reduced summer rainfall over eastern Asia and the western Pacific Warm Pool due to strengthened Walker circulation over the northern tropical Pacific. In boreal winter, though vertical motion increased over India, large parts of Asia experienced anomalous subsidence. In the SH, stronger vertical motion and enhanced water vapor transport were simulated in the monsoon region (Figure 9d). In general, the NH monsoon rainfall decreased and the SH experienced more monsoon rainfall in both seasons. The −0.2 Sv case showed different and weaker responses. In both seasons, the NH experienced stronger upward motion at the 500 hPa level in East Asian and African monsoon regions and water vapor converged toward monsoon regions whereas in the SH water vapor was mostly transported away from the monsoon regions accompanied by weaker vertical motion (Figures 9e and 9f).

Overall, based on our results, the AMOC strength showed a strong nonlinear behavior to freshwater perturbation and AMOC strength variations induced nonlinear responses in surface conditions including monsoon precipitation (annually and seasonally) corresponding to cold stadial and warm interstadial conditions. Our simulated ITCZ latitude shift in response to cross equatorial atmospheric heat transport change is about −3°/PW, which is comparable to the PMIP2 Last Glacial Maximum ensemble mean (Donohoe et al., 2013). The seasonal cycle of ITCZ latitude as function of cross equatorial atmospheric heat transport and meridional SST contrast also

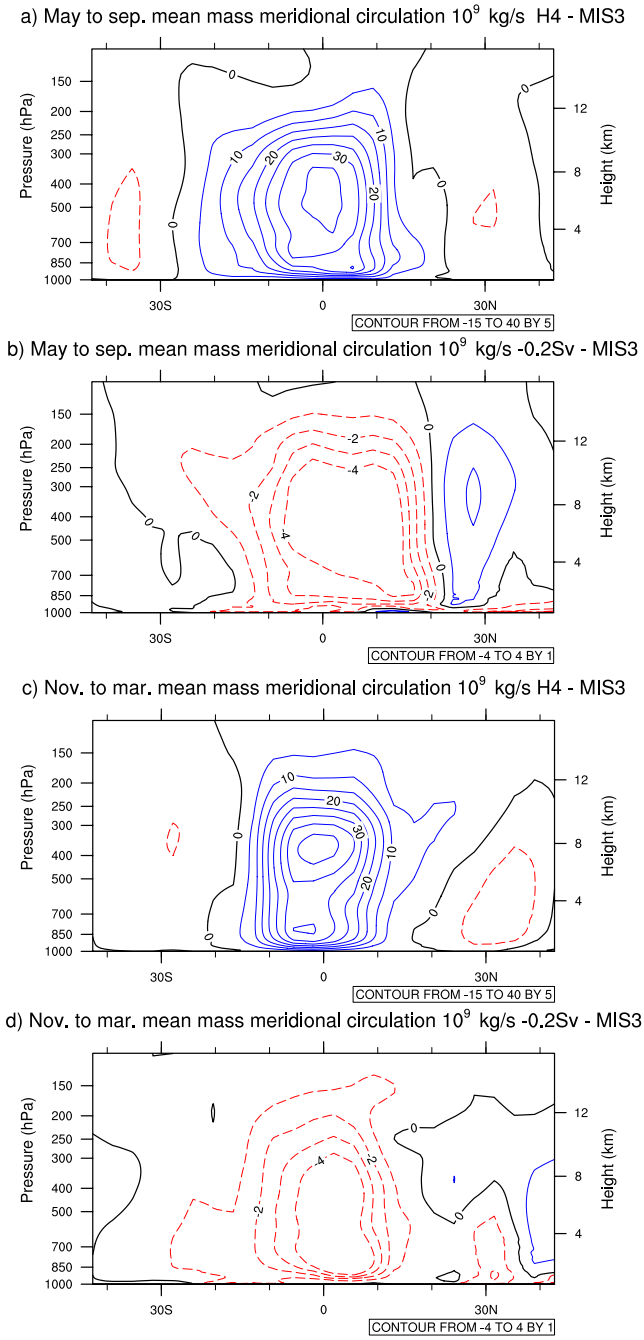

Figure 8. *Mean meridional mass streamfunction differences*. (a) +0.2 Sv–MIS3 control run (May to September); (b) −0.2 Sv–MIS3 control run (May to September); (c) same as (a) but for November to March; and (d) same as (b) but for November to March. Positive values indicate clockwise circulation and negative values indicate counterclockwise circulation.

matches the CMIP3 ensemble mean (McGee et al., 2014). Finally yet importantly, using other models to conduct similar experiments, which is beyond the scope of our present study could improve reliability of the study since there is large diversity in simulating glacial AMOC strength (Weber et al., 2007).

4. Conclusions

This study provides an integrated picture of global monsoon rainfall changes between cold stadials and mild interstadials during MIS3 by combining modeling results and proxies. The modeled monsoon rainfall variations are

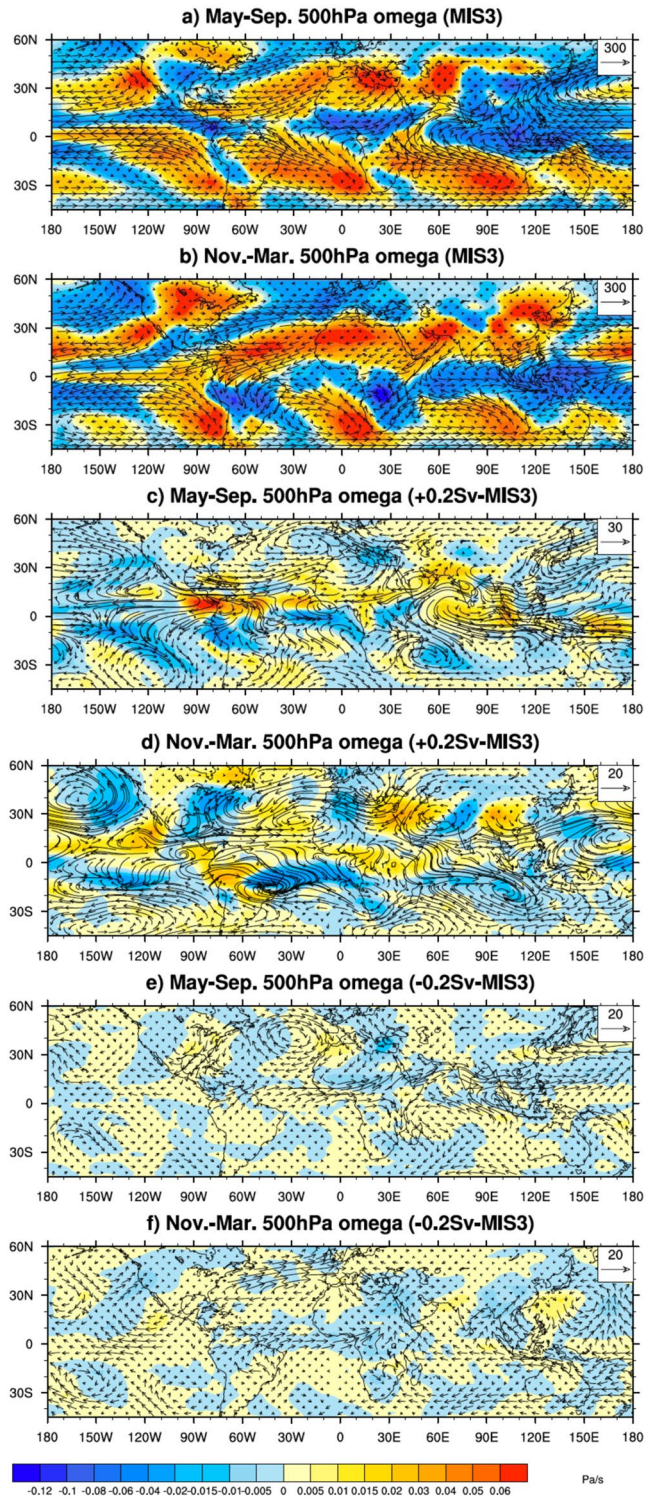

Figure 9. 1,000–500 hPa *water vapor flux and* 500 hPa Ω (*vertical pressure velocity*). (a) May to September mean in Marine Isotope Stage 3 (MIS3) control run; (b) November to March mean in MIS3 control run; (c) May to September difference between +0.2 Sv experiment and MIS3 control run; (d) same as (c) but for November to March; (e) same as (c) but for the −0.2 Sv experiment; and (f) same as (d) but for the −0.2 Sv experiment. Vector unit: kg/m/s and omega unit: Pa/s.

mostly consistent with proxy records. Such agreement provides further confidence in model simulations of global monsoon changes under climates different from the modern one and may aid the current monsoon research. We first recognize a nonlinearity in AMOC strength response to freshwater forcing in the North Atlantic, which mimics stadial and interstadial states in D-O oscillation. The global monsoon precipitation response to AMOC strength changes under MIS3 background climate was analyzed in detail. The most important finding of our study is that total annual and seasonal rainfall within the global monsoon region show a nonlinear response to freshwater induced AMOC changes. Corresponding to D-O cold phases (stadials), positive freshwater perturbations in the Nordic Seas slowed down the AMOC, decreased northward ocean heat transport, hence, cooled the NH and warmed the SH, which led to a more southward positioned ITCZ along with a more asymmetrical Hadley cell and an increase in annual global monsoon precipitation in the south and a decrease of monsoon rainfall in the north. A more vigorous Atlantic circulation induced by freshwater extraction did not have significant impact on monsoon rainfall globally and in the two hemispheres individually since the total oceanic heat transport was hardly affected. The bipolar seesaw pattern was much less significant, meridional SST contrast in the tropics limited and the ITCZ position stayed stable. As a result, the main factor affecting monsoon precipitation in the model is the oceanic heat transport between the hemispheres associated with the AMOC and the PMOC. Combining both model data and paleo records, our work showed a clear picture of global monsoon precipitation response to high latitude climate variations tied to abrupt climate oscillations during MIS3, which provides insight into high-low latitude teleconnections for both present and past climates.

Data Availability Statement

All model output used in this study (X. Zhang et al., 2023) including rainfall, AMOC strength, atmosphere velocity etc. could be found at https://doi.org/10.5281/zenodo.8412325. We have also included several NCL scripts used for this study in the same repository too.

Acknowledgments
Model simulations in this study were carried out at Der Norddeutsche Verbund für Hoch-und Höchstleistungsrechnen (HLRN) and supported by the National Natural Science Foundation of China (42172205, 2081011619301, and 42111530182), the PalMod project funded by the German Federal Ministry of Education and Science (BMBF), and the DFG Cluster of Excellence at MARUM. The authors whose names are listed certify that they have NO affiliations with or involvement in any organization or entity with any financial interest in the subject matter or materials discussed in this manuscript.

References

An, Z., Guoxiong, W., Jianping, L., Youbin, S., Yimin, L., Weijian, Z., et al. (2015). Global monsoon dynamics and climate change. *Annual Review of Earth and Planetary Sciences*, *43*(1), 29–77. https://doi.org/10.1146/annurev-earth-060313-054623

Andersen, K. K., Clausen, H. B., Dahl-Jensen, D., Gundestrup, N. S., Hvidberg, C. S., Johnsen, S. J., et al. (2004). High-resolution record of Northern Hemisphere climate extending into the last interglacial period. *Nature*, *431*(7005), 147–151. https://doi.org/10.1038/nature02805

Bakker, P., Schmittner, A., Lenaerts, J. T. M., Abe-Ouchi, A., Bi, D., van den Broeke, M. R., et al. (2016). Fate of the Atlantic meridional overturning circulation: Strong decline under continued warming and Greenland melting. *Geophysical Research Letters*, *43*(23), 12252–12260. https://doi.org/10.1002/2016GL070457

Beck, J. W., Zhou, W., Li, C., Wu, Z., White, L., Xian, F., et al. (2018). A 550,000-year record of East Asian monsoon rainfall from ^{10}Be in loess. *Science*, *360*(6391), 877–881. https://doi.org/10.1126/science.aam5825

Böhm, E., Lippold, J., Gutjahr, M., Frank, M., Blaser, P., Antz, B., et al. (2014). Strong and deep Atlantic meridional overturning circulation during the last glacial cycle. *Nature*, *517*(7532), 73–76. https://doi.org/10.1038/nature14059

Cai, Y. J., An, Z., Cheng, H., Edwards, R. L., Kelly, M. J., Liu, W., et al. (2006). High-resolution absolute-dated Indian Monsoon record between 53 and 36 ka from Xiaobailong Cave, southwestern China. *Geology*, *34*(8), 621–624. https://doi.org/10.1130/g22567.1

Cai, Y. J., Fung, I. Y., Edwards, R. L., An, Z., Cheng, H., Lee, J. E., et al. (2015). Variability of stalagmite-inferred Indian monsoon precipitation over the past 252,000 y. *Proceedings of the National Academy of Sciences of the United States of America*, *112*(10), 2954–2959. https://doi.org/10.1073/pnas.1424035112

Campos, M. C., Chiessi, C. M., Prange, M., Mulitza, S., Kuhnert, H., Paul, A., et al. (2019). A new mechanism for millennial scale positive precipitation anomalies over tropical South America. *Quaternary Science Reviews*, *225*, 105990. https://doi.org/10.1016/j.quascirev.2019.105990

Cheng, H., Edwards, R. L., Broecker, W. S., Denton, G. H., Kong, X., Wang, Y., et al. (2009). Ice age terminations. *Science*, *326*(5950), 248–252. https://doi.org/10.1126/science.1177840

Cheng, H., Sinha, A., Cruz, F. W., Wang, X., Edwards, R. L., d'Horta, F. M., et al. (2013). Climate change patterns in Amazonia and biodiversity. *Nature Communications*, *4*(1), 1411. https://doi.org/10.1038/ncomms2415

Cheng, H., Sinha, A., Wang, X., Cruz, F. W., & Edwards, R. L. (2012). The global paleomonsoon as seen through speleothem records from Asia and the Americas. *Climate Dynamics*, *39*(5), 1045–1062. https://doi.org/10.1007/s00382-012-1363-7

Chiang, C. H., Fung, I. Y., Wu, C. H., Cai, Y., Edman, J. P., Liu, Y., et al. (2015). Role of seasonal transitions and westerly jets in East Asian paleoclimate. *Quaternary Science Reviews*, *108*, 111–129. https://doi.org/10.1016/j.quascirev.2014.11.009

Chiang, J., Biasutti, M., & Battisti, D. (2003). Sensitivity of the Atlantic intertropical convergence zone to last glacial maximum boundary conditions. *Paleoceanography*, *18*(4), 1094. https://doi.org/10.1029/2003pa000916

Chiang, J. C., Herman, M. J., Yoshimura, K., & Fung, I. Y. (2020). Enriched East Asian oxygen isotope of precipitation indicates reduced summer seasonality in regional climate and westerlies. *Proceedings of the National Academy of Sciences of the United States of America*, *117*(26), 14745–14750. https://doi.org/10.1073/pnas.1922602117

Chiang, J. C. H., & Friedman, A. R. (2012). Extratropical cooling, interhemispheric thermal gradients, and tropical climate change. *Annual Review of Earth and Planetary Sciences*, *40*(1), 383–412. https://doi.org/10.1146/annurev-earth-042711-105545

Collins, D. W., Bitz, C. M., Blackmon, M. L., Bonan, G. B., Bretherton, C. S., Carton, J. A., et al. (2006). The community climate system model version 3 (CCSM3). *Journal of Climate*, *19*(11), 2122–2143. https://doi.org/10.1175/jcli3761.1

Deplazes, G., Lückge, A., Peterson, L. C., Timmermann, A., Hamann, Y., Hughen, K. A., et al. (2016). Links between tropical rainfall and North Atlantic climate during the last glacial period. *Nature Geoscience*, *6*(3), 213–217. https://doi.org/10.1038/NGEO1712

Donohoe, A., Marshall, J., Ferreira, D., & M1cGee, D. (2013). The relationship between ITCZ location and cross-equatorial atmospheric heat transport: From the seasonal cycle to the last glacial maximum. *Journal of Climate*, *26*(11), 3597–3618. https://doi.org/10.1175/jcli-d-12-00467.1

Elliot, M., Labeyrie, L., Dokken, T., & Manthé, S. (2001). Coherent patterns of ice-rafted debris deposits in the Nordic regions during the last glacial (10-60 ka). *Earth and Planetary Science Letters*, *194*(1–2), 151–163. https://doi.org/10.1016/s0012-821x(01)00561-1

Elliot, M., Labeyrie, L., & Duplessy, J. C. (2002). Changes in North Atlantic deep-water formation associated with the Dansgaard–Oeschger temperature oscillations (60–10 ka). *Quaternary Science Reviews*, *21*(10), 1153–1165. https://doi.org/10.1016/s0277-3791(01)00137-8

Frierson, D. M. W., Hwang, Y. T., Fučkar, N. S., Seager, R., Kang, S. M., Donohoe, A., et al. (2013). Contribution of ocean overturning circulation to tropical rainfall peak in the Northern Hemisphere. *Nature Geoscience*, *6*(11), 940–944. https://doi.org/10.1038/ngeo1987

Ganachaud, A., & Wunsch, C. (2000). Improved estimates of global ocean circulation, heat transport and mixing from hydrographic data. *Nature*, *408*(6811), 453–457. https://doi.org/10.1038/35044048

Guo, Z. T., Liu, T., Guiot, J., Wu, N., Lü, H., Han, J., et al. (1996). High frequency pulses of East Asian monsoon climate in the last two glaciations: Link with the North Atlantic. *Climate Dynamics*, *12*(10), 701–709. https://doi.org/10.1007/s003820050137

Hofmann, M., & Rahmstorf, S. (2009). On the stability of the Atlantic meridional overturning circulation. *Proceedings of the National Academy of Sciences of the United States of America*, *106*(49), 20584–20589. https://doi.org/10.1073/pnas.0909146106

Jackson, L., & Wood, R. A. (2018). Hysteresis and resilience of the AMOC in an eddy-permitting GCM. *Geophysical Research Letters*, *45*(16), 8547–8556. https://doi.org/10.1029/2018gl078104

Kanner, L. C., Burns, S. J., Cheng, H., & Edwards, R. L. (2012). High latitude forcing of the South American summer monsoon during the last glacial. *Science*, *335*(6068), 570–573. https://doi.org/10.1126/science.1213397

Lau, N. C., & Nath, M. J. (2000). Impact of ENSO on the variability of the Asian–Australian monsoons as simulated in GCM experiments. *Journal of Climate*, *13*(24), 4287–4309. https://doi.org/10.1175/1520-0442(2000)013<4287:ioeotv>2.0.co;2

McGee, D., Donohoe, A., Marshall, J., & Ferreira, D. (2014). Changes in ITCZ location and cross-equatorial heat transport at the last glacial maximum, Heinrich Stadial 1, and the mid-Holocene. *Earth and Planetary Science Letters*, *390*, 69–79. https://doi.org/10.1016/j.epsl.2013.12.043

Mohtadi, M., Prange, M., & Steinke, S. (2016). Palaeoclimatic insights into forcing and response of monsoon rainfall. *Nature*, *533*(7602), 191–199. https://doi.org/10.1038/nature17450

Mulitza, S., Prange, M., Stuut, J., Zabel, M., von Dobeneck, T., Itambi, A. C., et al. (2008). Sahel megadroughts triggered by glacial slowdowns of Atlantic meridional overturning. *Paleoceanography*, *23*(4), PA4206. https://doi.org/10.1029/2008pa001637

Orland, I. J., Edwards, R. L., Cheng, H., Kozdon, R., Cross, M., & Valley, J. W. (2015). Direct measurements of deglacial monsoon strength in a Chinese stalagmite. *Geology*, *43*(6), 555–558. https://doi.org/10.1130/g36612.1

Otto-Bliesner, B. L., Russell, J. M., Clark, P. U., Liu, Z., Overpeck, J. T., Konecky, B., et al. (2014). Coherent changes of southeastern equatorial and northern African rainfall during the last deglaciation. *Science*, *346*(6214), 1223–1227. https://doi.org/10.1126/science.1259531

Pierrehumbert, R. T. (2000). Climate change and the tropical Pacific: The sleeping dragon wakes. *Proceedings of the National Academy of Sciences of the United States of America*, *97*(4), 1355–1358. https://doi.org/10.1073/pnas.97.4.1355

Praetorius, S. K. (2018). North Atlantic circulation slows down. *Nature*, *556*(7700), 180–181. https://doi.org/10.1038/s41586-018-0006-5

Prange, M., Lohmann, G., & Paul, A. (2003). Influence of vertical mixing on the thermohaline hysteresis: Analyses of an OGCM. *Journal of Physical Oceanography*, *33*(8), 1707–1721. https://doi.org/10.1175/2389.1

Rachmayani, R., Prange, M., & Schulz, M. (2015). North African vegetation-precipitation feedback in early and mid-Holocene climate simulations with CCSM3-DGVM. *Climate of the Past*, *11*(2), 175–185. https://doi.org/10.5194/cp-11-175-2015

Saenko, O. A., Schmittner, A., & Weaver, A. J. (2004). The Atlantic–Pacific seesaw. *Journal of Climate*, *17*(11), 2033–2038. https://doi.org/10.1175/1520-0442(2004)017<2033:tas>2.0.co;2

Schulz, M. (2002). On the 1470-year pacing of Dansgaard-Oeschger warm events. *Paleoceanography*, *17*(2), 4-1–4-9. https://doi.org/10.1029/2000PA000571

Smith, R. D., Kortas, S., & Meltz, B. (1995). *Curvilinear coordinates for global ocean models. Tech. Rep. LA-UR-95-1146* (p. 50). Los Alamos National Laboratory.

Stocker, T. F., & Johnsen, S. J. (2003). A minimum thermodynamic model for the bipolar seesaw. *Paleoceanography*, *18*(4), 1087. https://doi.org/10.1029/2003pa000920

Stouffer, R. J., Yin, J., Gregory, J. M., Kamenkovich, I. V., Sokolov, A., Hurlin, W., et al. (2006). Investigating the causes of the response of the thermohaline circulation to past and future climate changes. *Journal of Climate*, *19*(8), 1365–1387. https://doi.org/10.1175/jcli3689.1

Stríkis, N. M., Cruz, F. W., Barreto, E. A. S., Naughton, F., Vuille, M., Cheng, H., et al. (2018). South American monsoon response to iceberg discharge in the North Atlantic. *Proceedings of the National Academy of Sciences of the United States of America*, *115*(15), 3788–3793. https://doi.org/10.1073/pnas.1717784115

Sun, Y. B., Clemens, S. C., Morrill, C., Lin, X., Wang, X., & An, Z. (2012). Influence of Atlantic meridional overturning circulation on the East Asian winter monsoon. *Nature Geoscience*, *5*(1), 46–49. https://doi.org/10.1038/ngeo1326

Sun, Y. B., McManus, J. F., Clemens, S. C., Zhang, X., Vogel, H., Hodell, D. A., et al. (2021). Persistent orbital influence on millennial climate variability through the Pleistocene. *Nature Geoscience*, *14*(11), 812–818. https://doi.org/10.1038/s41561-021-00794-1

Sun, Y. B., Yin, Q., Crucifix, M., Clemens, S. C., Araya-Melo, P., Liu, W., et al. (2019). Diverse manifestations of the Mid-Pleistocene climate transition. *Nature Communications*, *10*(1), 352. https://doi.org/10.1038/s41467-018-08257-9

Voelker, A. H. L. (2002). Global distribution of centennial-scale records for marine isotope stage (MIS) 3: A database. *Quaternary Science Reviews*, *21*(10), 1185–1212. https://doi.org/10.1016/s0277-3791(01)00139-1

Wang, P. X., Wang, B., Cheng, H., Fasullo, J., Guo, Z. T., Kiefer, T., & Liu, Z. Y. (2014). The global monsoon across timescales: Coherent variability of regional monsoons. *Climate of the Past*, *10*(6), 2007–2052. https://doi.org/10.5194/cp-10-2007-2014

Wang, X., Auler, A., Edwards, R., Cheng, H., Cristalli, P. S., Smart, P. L., et al. (2004). Wet periods in northeastern Brazil over the past 210 kyr linked to distant climate anomalies. *Nature*, *432*(7018), 740–743. https://doi.org/10.1038/nature03067

Wang, X., Auler, A. S., Edwards, R. L., Cheng, H., Ito, E., & Solheid, M. (2006). Interhemispheric anti-phasing of rainfall during the last glacial period. *Quaternary Science Reviews*, *25*(23–24), 3391–3403. https://doi.org/10.1016/j.quascirev.2006.02.009

Wang, X., Auler, A. S., Edwards, R. L., Cheng, H., Ito, E., Wang, Y., et al. (2007). Millennial-scale precipitation changes in southern Brazil over the past 90 000 years. *Geophysical Research Letters*, *34*(23), L23701. https://doi.org/10.1029/2007GL031149

Wang, Y. J., Cheng, H., Edwards, R. L., An, Z. S., Wu, J. Y., Shen, C. C., & Dorale, J. A. (2001). A high-resolution absolute-dated Late Pleistocene monsoon record from Hulu Cave, China. *Science*, *294*(5550), 2345–2348. https://doi.org/10.1126/science.1064618

Wang, Y. J., Cheng, H., Edwards, R. L., Kong, X., Shao, X., Chen, S., et al. (2008). Millennial- and orbital-scale changes in the East Asian monsoon over the past 224,000 years. *Nature*, *28*(7182), 1090–1093. https://doi.org/10.1038/nature06692

Weber, S. L., Drijfhout, S. S., Abe-Ouchi, A., Crucifix, M., Eby, M., Ganopolski, A., et al. (2007). The modern and glacial overturning circulation in the Atlantic Ocean in PMIP coupled model simulations. *Climate of the Past*, *3*(1), 51–64. https://doi.org/10.5194/cp-3-51-2007

Webster, P. J. (1994). The role of hydrological processes in ocean-atmosphere interactions. *Reviews of Geophysics*, *32*(4), 427–476. https://doi.org/10.1029/94rg01873

Wen, X., Liu, Z., Wang, S., Cheng, J., & Zhu, J. (2016). Correlation and anti-correlation of the East Asian summer and winter monsoons during the last 21,000 years. *Nature Communications*, *7*(1), 11999. https://doi.org/10.1038/ncomms11999

Yan, M., Wang, B., & Liu, J. (2016). Global monsoon change during the last glacial maximum: A multi-model study. *Climate Dynamics*, *47*(1–2), 359–374. https://doi.org/10.1007/s00382-015-2841-5

Yeager, S. G., Shields, C. A., Large, W. G., & Hack, J. J. (2006). The low-resolution CCSM3. *Journal of Climate*, *19*(11), 2545–2566. https://doi.org/10.1175/jcli3744.1

Zhang, R., & Delworth, T. (2005). Simulated tropical response to a substantial weakening of the Atlantic thermohaline circulation. *Journal of Climate*, *18*(12), 1853–1860. https://doi.org/10.1175/jcli3460.1

Zhang, X., & Prange, M. (2020). Stability of the Atlantic overturning circulation under intermediate (MIS3) and full glacial (LGM) conditions and its relationship with Dansgaard-Oeschger climate variability. *Quaternary Science Reviews*, *242*, 106443. https://doi.org/10.1016/j.quascirev.2020.106443

Zhang, X., Prange, M., Ma, L., & Liu, J. (2023). Nonlinear response of global monsoon precipitation to Atlantic overturning strength variations during Marine Isotope Stage 3. *Zenodo*. https://doi.org/10.5281/zenodo.8412325

Zhang, X., Prange, M., Merkel, U., & Schulz, M. (2014). Instability of the Atlantic overturning circulation during marine isotope stage 3. *Geophysical Research Letters*, *41*(12), 4285–4293. https://doi.org/10.1002/2014gl060321

Zhang, X., Prange, M., Merkel, U., & Schulz, M. (2015). Spatial fingerprint and magnitude of changes in the Atlantic meridional overturning circulation during Marine Isotope Stage 3. *Geophysical Research Letters*, *42*(6), 1903–1911. https://doi.org/10.1002/2014gl063003

Zhang, Z., Licht, A., De Vleeschouwer, D., Wang, Z., Li, Y., Kemp, D. B., et al. (2022). East Asian monsoonal climate sensitivity changed in the late Pliocene in response to northern hemisphere glaciations. *Geophysical Research Letters*, *49*(23), e2022GL101280. https://doi.org/10.1029/2022gl101280

Zhao, Y., Tzedakis, P. C., Li, Q., Qin, F., Cui, Q., Liang, C., et al. (2020). Evolution of vegetation and climate variability on the Tibetan Plateau over the past 1.74 million years. *Science Advances*, *6*(19), eaay6193. https://doi.org/10.1126/sciadv.aay6193

Zhou, H., Zhao, J. X., Feng, Y., Chen, Q., Mi, X., Shen, C. C., et al. (2014). Heinrich event 4 and Dansgaard/Oeschger events 5–10 recorded by high-resolution speleothem oxygen isotope data from central China. *Quaternary Research*, *82*(2), 394–404. https://doi.org/10.1016/j.yqres.2014.07.006

Ziegler, M., Simon, M. H., Hall, I. R., Barker, S., Stringer, C., & Zahn, R. (2013). Development of Middle Stone Age innovation linked to rapid climate change. *Nature Communications*, *4*(1), 1905. https://doi.org/10.1038/ncomms2897